Phonon Energy Gaps in the Charged Incommensurate Planes of the Spin-Ladder $Sr_{14}Cu_{24}O_{41}$ Compound by Raman and Infrared Spectroscopy

V. K. Thorsmølle,[1,2,4,*] C. C. Homes,[3,†] A. Gozar,[3,‡] G. Blumberg,[4] J. L. M. van Mechelen,[2] A. B. Kuzmenko,[2] S. Vanishri,[5] C. Marin,[5] and H. M. Rønnow[6]

[1]*Laboratory for Photonics and Interfaces, École Polytechnique Fédérale de Lausanne (EPFL), CH-1015, Switzerland*
[2]*Département de Physique de la Matière Condensée, Université de Genève, CH-1211 Genève 4, Switzerland*
[3]*Condensed Matter Physics and Materials Science Department, Brookhaven National Laboratory, Upton, New York 11973, USA*
[4]*Department of Physics and Astronomy, Rutgers, The State University of New Jersey, Piscataway, New Jersey 08854, USA*
[5]*CEA Grenoble, INAC, SPSMS, IMAPEC, 17 rue des Martyrs, 38054 Grenoble, France*
[6]*Laboratory for Quantum Magnetism, École Polytechnique Fédérale de Lausanne (EPFL), CH-1015, Switzerland*

(Received 13 December 2011; published 21 May 2012)

The terahertz (THz) excitations in the quantum spin-ladder system $Sr_{14}Cu_{24}O_{41}$ have been determined along the c axis using THz time-domain, Raman, and infrared spectroscopy. Low-frequency infrared and Raman active modes are observed above and below the charge-ordering temperature $T_{co} \simeq 200$ K over a narrow interval $\simeq$ 1–2 meV ($\simeq$ 8–16 cm^{-1}). A new infrared mode at $\simeq$ 1 meV develops below $\simeq$ 100 K. The temperature dependence of these modes shows that they are coupled to the charge- and spin-density-wave correlations in this system. These low-energy features are conjectured to originate in the gapped sliding motion of the chain and ladder subsystems, which are both incommensurate and charged.

DOI: 10.1103/PhysRevLett.108.217401 PACS numbers: 78.30.−j, 71.45.Lr, 78.70.Gq

More than three decades ago, new normal modes were predicted to occur in ionic materials with incommensurate (IC) layers that can slide past each other [1–4]. These new degrees of freedom allow separate phonons in each subsystem at high frequencies with a crossover to slow oscillations due to relative sliding motions of the two almost rigid subsystems at ultralow frequencies, leading effectively to an extra acoustic mode. If the IC layers are charged these sliding modes become gapped due to the restoring Coulomb forces. These modes are the ionic complements of the electronic plasmons in metals and their dynamics also resemble the sliding motion in density wave (DW) systems [5]. Thus far, unambiguous experimental evidence for sliding gapped acoustic mode resonances has remained, to our knowledge, elusive. A promising avenue of investigation is the low-dimensional quantum spin-ladder system $Sr_{14}Cu_{24}O_{41}$ containing such substructures in the form of Cu_2O_3 ladders and one-dimensional CuO_2 chains [6]. The chains and ladders run parallel along the c axis with the rungs of the ladders along the a axis [6], shown in Fig. 1. The two subsystems are structurally IC, resulting in a buckling along the c axis with a period $c = 27.5$ Å $\simeq 10c_{ch} \simeq 7c_{ld}$, where c_{ch} and c_{ld} represent the lattice constants for the chain and ladder subcells, respectively.

This intrinsically hole-doped material exhibits a variety of unusual charge, magnetic and vibrational phenomena [7] that have been probed by several techniques, among them magnetic resonance [8], neutron scattering [9], and resonant x-ray scattering [10–12]. The unusual DW order is attributed to cooperative phenomena driven and stabilized by charge and spin correlations, in conjunction with the IC lattice degrees of freedom. Low-energy features spanning frequencies from the kHz to the THz range and associated with the DW dynamics have also been observed. However, while the microwave data have been consistently interpreted in terms of screened DW relaxational dynamics [13–16], the nature of the excitations in the THz regime, which are seen to be strongly coupled to the charge or spin ordering, remains controversial [10–19]. An important and open question is, what are the salient spectroscopic features in the $\simeq$ 1 meV energy region?

In this Letter we demonstrate using three experimental techniques that low-energy collective modes in $Sr_{14}Cu_{24}O_{41}$ consist of one Raman and one infrared (IR) active excitation present in the 5–300 K temperature region, as well as a new mode appearing well below the charge-ordering temperature ($T_{co} \simeq 200$ K) whose temperature-dependent behavior is tracked by terahertz time-domain spectroscopy (THz-TDS) [20]. An intuitive interpretation of these modes in relation to ''phononic gaps'' opened by Coulomb interactions in IC lattices and coupled to the DW ordering is able to consistently explain the range and relative energies of these excitations that are illustrated in Fig. 1.

Single crystals of $Sr_{14}Cu_{24}O_{41}$ were grown using the traveling-solvent floating-zone method. The sample was oriented and cut to 4×6 mm, with a thickness of 440 μm and the a and c axes in the plane. The THz-TDS experiments (TPI spectra 1000, TeraView Ltd.) were performed in transmission geometry with the sample mounted inside an optical cryostat capable of reaching 5 K. To obtain the complex conductivity and the transmittance window of the time-domain signals lasting beyond 60 ps (containing several Fabry-Perot internal sample reflections), a complete

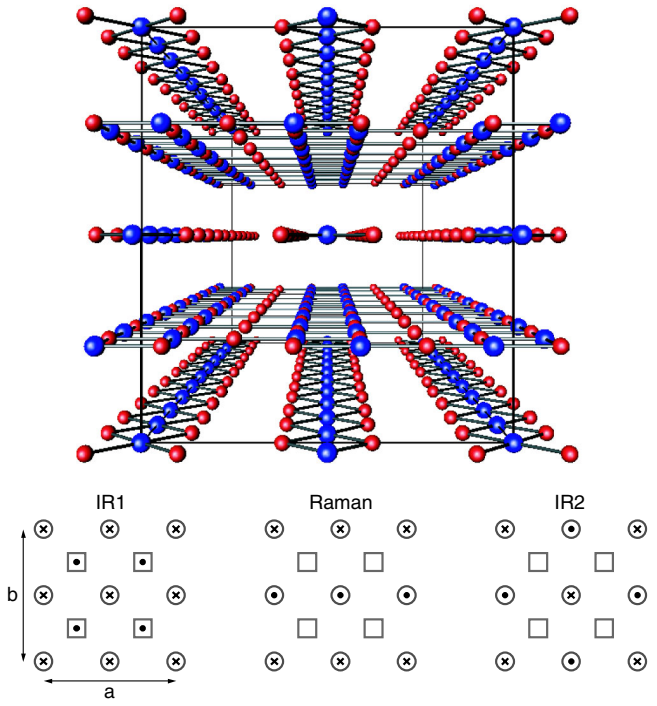

FIG. 1 (color online). Perspective view of the ideal unit cell of $Sr_{14}Cu_{24}O_{41}$ (the Sr atoms are omitted) in the a-b plane viewed along the c axis showing the stacking of the CuO_2 chains and the Cu_2O_3 ladders. Beneath the unit cell are the symbolic representations of the low-frequency infrared and Raman modes in the ladders and chains (see text for details); the chains are depicted by the circles ($q_{ch} \simeq -1.4e$), and the ladders by the squares ($q_{ld} \simeq 2e$). The dots and crosses refer to the oscillatory motion in and out of the a-b plane, respectively.

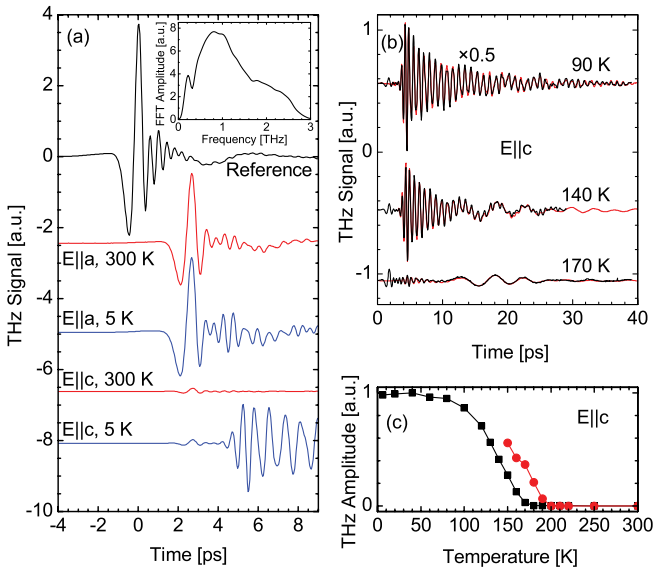

FIG. 2 (color online). Electric field $E(t)$ of THz pulse in the time-domain transmitted through a 440-μm thick $Sr_{14}Cu_{24}O_{41}$ crystal. (a) $E(t)$ polarized along the a and c axis at 300 and 5 K. The reference is recorded without the crystal. The inset shows the FFT amplitude spectrum of $E(t)$ for the reference. (b) $E(t)$ (black lines) along the c axis shown with the Drude-Lorentz time-domain fits (red lines) at three different temperatures. (c) Temperature dependence of the largest peak of the amplitude for the fast oscillation (black squares) and slow oscillation (red circles) of the THz signal. The slow oscillation is only shown to 150 K.

Drude-Lorentz time-domain analysis study is presented, in contrast to simple frequency inversion [21]. The polarized reflectance was measured over a wide frequency range using an *in situ* evaporation technique [22]. The complex conductivity is determined from a Kramers-Kronig analysis of the reflectance [23] requiring extrapolations in the $\omega \rightarrow 0$ limit; above 250 K a Hagen-Rubens form is employed $R(\omega) \propto 1 - \sqrt{\omega}$, while below this temperature the reflectance is assumed to be constant, $R(\omega \rightarrow 0) \simeq 0.68$–$0.76$. The Raman measurements were performed in cc and aa polarizations as described in Ref. [15]. The direction of propagation of the light was perpendicular to the a-c plane for all measurements.

Figure 2(a) shows the electric field of the THz pulse transmitted through the $Sr_{14}Cu_{24}O_{41}$ sample comparing the response for polarizations along the a and c axis at high and low temperatures, as well as a reference signal without a sample. The Fourier transformed (FFT) amplitude spectrum for the reference is shown in the inset. For the electric field polarized along the a axis, the shape of the THz pulse is essentially the same at 300 and 5 K, characteristic of insulating behavior along this direction. However, for the electric field polarized along the c axis, the THz signal is barely present at 300 K, indicative of metallic response at higher temperatures. At low temperatures a distinct long-lived ringing is observed with a period of $\simeq 1$ ps. Figure 2(b) shows the transmitted THz pulse polarized along the c axis for three different temperatures with time-domain fits revealing an additional $\simeq 4$ ps oscillation. The $\simeq 4$ ps period oscillation is observed to appear below $\simeq 200$ K, while the $\simeq 1$ ps oscillation below $\simeq 170$ K, as shown in Fig. 2(c).

The far-infrared reflectance for light polarized along the c axis is shown in Fig. 3(a), while (b) shows the transmittance for the electric field polarized along the c axis of the THz oscillations presented in Fig. 2; Figs. 3(c) and 3(d) show the aa and cc Raman responses, respectively [24]. A metallic Drude-like behavior is observed in the reflectance above T_{co}. For $T \lesssim T_{co}$ the reflectance changes from a metallic to an insulating character, allowing a strong vibrational feature to emerge. For the transmittance shown in Fig. 3(b) there is a sharply defined window where the transmittance is effectively blocked by at least 5 orders of magnitude between $\simeq$ 13–33 cm^{-1} (1 meV $\simeq 8.1$ cm^{-1}, 1 THz $\simeq 33.3$ cm^{-1}), corresponding to the pronounced slow and fast oscillations observed in the time-domain (Fig. 2). As the temperature is raised, the upper limit of this window becomes less effective until $T \gtrsim T_{co}$, at which point the entire region becomes increasingly opaque. In addition, one also notices an absorption at $\simeq 8$ cm^{-1} that also decreases with increasing

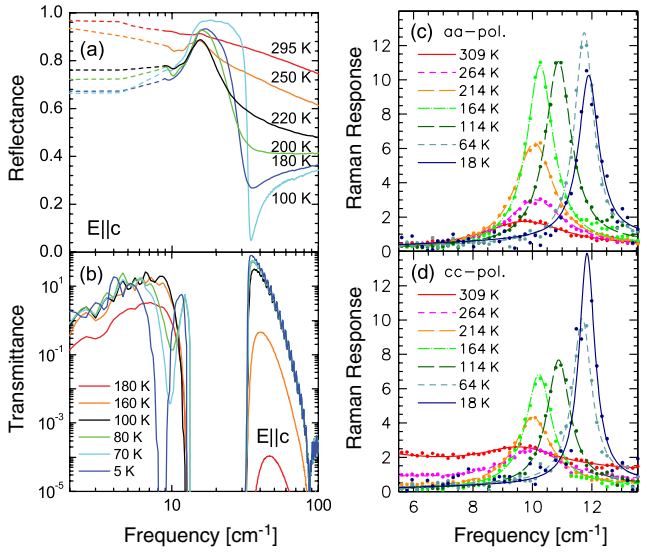

FIG. 3 (color online). (a) Infrared reflectance of $Sr_{14}Cu_{24}O_{41}$ for light polarized along the c axis above and below T_{co} where the dashed lines indicate the $\omega \rightarrow 0$ extrapolations. (b) Transmittance for light polarized along the c axis ($T \lesssim T_{co}$). (c) Raman response in relative units for the aa polarization. (d) cc polarization at various temperatures. The Raman data were adapted from Ref. [24].

temperature. The loss of the electronic background for $T \lesssim T_{co}$ signals the transition to a DW ground state and an insulating phase.

Figure 4(a) shows the temperature dependence of the real part of the optical conductivity along the c axis. A metallic response is observed for $T \gtrsim T_{co}$, while for $T \lesssim T_{co}$ an insulating response develops. The mode at 14.9 cm^{-1} narrows and softens to 12.6 cm^{-1} at low temperature with a slight kink around T_{co} (we refer to this mode as IR1). The Raman mode seen in aa and cc polarizations has the opposite behavior; its position increases from 9.5 to 12 cm^{-1} upon cooling from $\simeq 300$ to 5 K. Interestingly, below T_{co}, a new infrared mode branches off below 10 cm^{-1} towards lower frequencies, reaching 8.4 cm^{-1} at $\simeq 5$ K; the temperature dependence of this new mode (which we denote IR2) closely resembles the behavior reported for the weakly dispersive magnetic chain excitations [9]. Along the a axis the optical conductivity is an order of magnitude smaller than it is along the c axis, confirming the insulating behavior perpendicular to the chains and ladders (not shown); in addition to a number of weak features, a sharp infrared phonon is observed at $\simeq 57$ cm^{-1}. The remaining panels in Fig. 4 show the details of the c axis features in the optical conductivity with (b) a contour plot of optical conductivity as a function of frequency and temperature; (c) the frequency of IR1 and IR2, as well as the frequency of the aa and cc Raman excitations, their respective (d) strengths and (e) linewidths. We note that the total oscillator strength of IR1 and IR2 appears to be conserved [Fig. 4(d)].

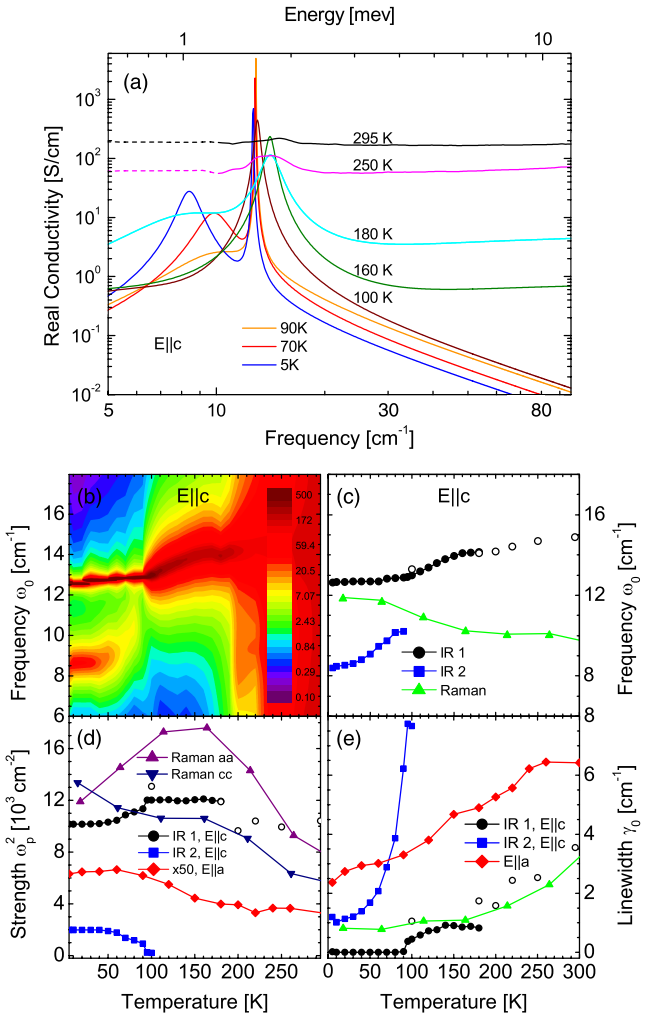

FIG. 4 (color online). (a) THz-TDS conductivity along the c axis of $Sr_{14}Cu_{24}O_{41}$ above and below T_{co}. Above 180 K the conductivity was calculated from the reflectance (see text); the dashed lines indicate where the conductivity has been determined from the extrapolations supplied for the reflectance [Fig. 2(a)]. (b) Contour plot of the conductivity along the c axis as a function of frequency and temperature. (c) Temperature dependence of the two phonon modes observed in (a) shown together with the Raman active mode [Figs. 3(c) and 3(d)]. The strengths and linewidths are shown in (d) and (e), respectively, together with that of the a-axis phonon mode at $\simeq 57$ cm^{-1}. The amplitudes of the Raman data in (d) is in arbitrary units. The open symbols indicate data obtained from reflectance measurements.

It is tempting to relate these excitations to folded phonon modes due to the 10/7 superstructure. However, using $c \simeq 27.5$ Å and the sound velocity $v_s \simeq 13$ km/s [25], one would expect these excitations at energies $\simeq 100$ cm^{-1}. This is a factor of 10 higher than what we observe suggesting that a different mechanism is at work.

We then turn our attention to the scenario of the sliding motions of the chain and ladder subsystems presented in Fig. 1. The energy scale and the relative frequencies of the Raman and IR1 modes can be understood qualitatively

by taking into account the c axis incommensurability between the chain and ladder unit cells, $c_{ch}/c_{ld} \simeq 0.699$, in accordance with recent x-ray studies [26,27] that demonstrated that consideration of the super space group is mandatory. We assign n, m, and q to the corresponding atomic mass density, unit-cell mass, and charge, respectively. Using the available crystallographic data we obtain without any fitting parameters

$$\omega_{IR1} = \sqrt{\frac{n_{ch} q_{ch}^2}{\varepsilon_0 \varepsilon_\infty m_{ch}} \left(1 + \frac{c_{ld}}{c_{ch}} \frac{m_{ch}}{m_{ld}}\right)} \simeq 29.5 \text{ cm}^{-1} \quad (1)$$

for IR1 [2]. Here the chains and ladders are considered uniformly charged and $\varepsilon_\infty(75 \text{ cm}^{-1}) \simeq 15$ is the experimentally measured contribution of all other higher-energy phonons to the dielectric permittivity. All holes were assumed to be located in the chain system, i.e. $q_{ch} = -1.4e$ and $q_{ld} = 2e$. This is the ionic complement of the electronic zone-center plasmons in metals. In general this mode is acoustic with a diffusive character at long wavelengths, but it becomes gapped due to restoring Coulomb forces if the IC systems are oppositely charged [1–4]. The Raman mode corresponds to the out-of-phase oscillation of the chain layers, phase shifted by π along the b axis, with the ladders at rest (Fig. 1). Its frequency can be estimated by Eq. (1) in the $m_{ld} \to \infty$ limit. Hence, $\omega_R \simeq 0.85\omega_{IR1}$, which is in good agreement with the experimental observations. Removal of free carriers with decreasing temperature due to the activated nature of the conductivity would reduce screening effects, leading to the Raman mode hardening at low temperatures, also in agreement with our observations.

We suggest that the origin and energy of the IR2 mode can be understood by considering the effects of quasi-2D charge ordering in the chains [9]. Once the long-range hole ordering in the chains sets in below $\simeq 100$ K, restoring Coulomb forces will oppose the out-of-phase oscillation of adjacent chains. Above 100 K this excitation is expected to have a vanishingly small energy because of the short-range charge correlations along the a axis resulting in the absence of net restoring electrostatic forces in the disordered state. For a long-range sinusoidal charge modulation, the energy of this mode is

$$\omega_{IR2}^2 \propto \sqrt{\frac{\lambda}{\pi d}} \exp\left(-\frac{\pi d}{\lambda}\right) \frac{\delta q^2}{m_{ch} c_{ch} \lambda^2}, \quad (2)$$

with a proportionality factor of the order of unity. Here d, λ, and δq are the distance between two chains, the wavelength, and depth of the harmonic charge modulation, respectively. In $Sr_{14}Cu_{24}O_{41}$ this charge modulation is not a simple sinusoid; however, to first order a harmonic approximation may be used for two coupled chains. Taking $\lambda \simeq 5c_{ch}$, $d \simeq 5.7$ Å, and an average charge modulation depth $\langle \delta q \rangle \simeq 0.37e$, we find $\omega_{IR2} \approx 3 \text{ cm}^{-1}$, again consistent with the experimental data. From Eq. (2) it is seen that IR2 is a direct probe of the charge order. The situation is quite similar to undoped $La_6Ca_8Cu_{24}O_{41}$ where the staggered chain arrangement along the a axis should generate restoring Coulomb forces π-shifted oscillations of adjacent chains, and the analog of the IR2 mode in $Sr_{14}Cu_{24}O_{41}$ is expected to be present at all temperatures. This is in agreement with our experimental observations. A quantitative analysis of the IR2 mode and comparison to crystals of the "14-24-41" family will be the topic of a future study.

In conclusion, we propose that the low-energy Raman and IR1 excitations in $Sr_{14}Cu_{24}O_{41}$ originate from sliding motions of the IC chains and ladders that are gapped by Coulomb interactions due to the net charge carried by these subsystems. Long-range charge ordering in the chains will further generate low-energy infrared activity, and we suggest this to be at the origin of the new IR2 mode observed in the time-domain THz data below $\simeq 100$ K. The energy of this mode is as such a direct probe of the charge modulation depth as well as of the quasi-2D hole ordering pattern in the chain subsystem.

We gratefully acknowledge useful discussions with T. Maurice Rice and Jason Hancock. We would like to thank H. Eisaki for providing us with samples. Work at Brookhaven was supported by the U.S. Department of Energy, Office of Basic Energy Sciences, Division of Materials Sciences and Engineering under Contract No. DE-AC02-98CH10886. Work at Rutgers was supported by NSF DMR-1104884. Thanks to Professor H. L. Bhat of IISc, Bangalore for the Indo-French collaborative project, CEFIPRA under project No. 3408-4, which supported the crystal growth work at CEA Grenoble. A. G. acknowledges support from the Early Career Research Program (Grant No. 2005410).

*vernerkt@physics.rutgers.edu
†homes@bnl.gov
‡agozar@bnl.gov

[1] G. Theodorou and T. M. Rice, Phys. Rev. B **18**, 2840 (1978).
[2] G. Theodorou, Solid State Commun. **33**, 561 (1980).
[3] J. D. Axe and P. Bak, Phys. Rev. B **26**, 4963 (1982).
[4] W. Finger and T. M. Rice, Phys. Rev. B **28**, 340 (1983).
[5] G. Grüner, *Density Waves in Solids* (Addison-Wesley, Reading, MA, 1994).
[6] E. M. McCarron, III, M. A. Subramanian, J. C. Calabrese, and R. L. Harlow, Mater. Res. Bull. **23**, 1355 (1988); T. Siegrist, L. Schneemeyer, S. Sunshine, J. Waszczak, and R. Roth, *ibid.* **23**, 1429 (1988).
[7] T. Vuletić, B. Korin-Hamzić, T. Ivek, S. Tomić, B. Gorshunov, M. Dressel, and J. Akimitsu, Phys. Rep. **428**, 169 (2006).
[8] M. Takigawa, N. Motoyama, H. Eisaki, and S. Uchida, Phys. Rev. B **57**, 1124 (1998).
[9] M. Matsuda, T. Yosihama, K. Kakurai, and G. Shirane, Phys. Rev. B **59**, 1060 (1999).

[10] P. Abbamonte, G. Blumberg, A. Rusydi, A. Gozar, P. G. Evans, T. Siegrist, L. Venema, H. Eisaki, E. D. Isaacs, and G. A. Sawatzky, Nature (London) **431**, 1078 (2004).
[11] A. Rusydi, P. Abbamonte, H. Eisaki, Y. Fujimaki, G. Blumberg, S. Uchida, and G. A. Sawatzky, Phys. Rev. Lett. **97**, 016403 (2006).
[12] A. Rusydi, P. Abbamonte, H. Eisaki, Y. Fujimaki, S. Smadici, N. Motoyama, S. Uchida, Y.-J. Kim, M. Rübhausen, and G. A. Sawatzky, Phys. Rev. Lett. **100**, 036403 (2008).
[13] G. Blumberg, P. Littlewood, A. Gozar, B. S. Dennis, N. Motoyama, H. Eisaki, and S. Uchida, Science **297**, 584 (2002).
[14] B. Gorshunov, P. Haas, T. Rõõm, M. Dressel, T. T. Vuletić, B. Korin-Hamzić, S. Tomić, J. Akimitsu, and T. Nagata, Phys. Rev. B **66**, 060508(R) (2002).
[15] A. Gozar, G. Blumberg, P. B. Littlewood, B. S. Dennis, N. Motoyama, H. Eisaki, and S. Uchida, Phys. Rev. Lett. **91**, 087401 (2003).
[16] T. Vuletić, B. Korin-Hamzić, S. Tomić, B. Gorshunov, P. Haas, T. Rõõm, M. Dressel, J. Akimitsu, T. Sasaki, and T. Nagata, Phys. Rev. Lett. **90**, 257002 (2003).
[17] T. Vuletić, T. Ivek, B. Korin-Hamzić, S. Tomić, B. Gorshunov, P. Haas, M. Dressel, J. Akimitsu, T. Sasaki, and T. Nagata, Phys. Rev. B **71**, 012508 (2005).
[18] K.-Y. Choi, M. Grove, P. Lemmens, M. Fischer, G. Güntherodt, U. Ammerahl, B. Büchner, G. Dhalenne, A. Revcolevschi, and J. Akimitsu, Phys. Rev. B **73**, 104428 (2006).
[19] A. Rusydi, M. Berciu, P. Abbamonte, S. Smadici, H. Eisaki, Y. Fujimaki, S. Uchida, M. Rübhausen, and G. A. Sawatzky, Phys. Rev. B **75**, 104510 (2007).
[20] V. K. Thorsmølle, B. Wenger, J. Teuscher, J. C. Bauer, and J.-E. Moser, Chimia **61**, 631 (2007).
[21] J. C. Brauer, V. K. Thorsmølle, and J.-E. Moser, Chimia **63**, 189 (2009).
[22] C. C. Homes, M. Reedyk, D. A. Crandles, and T. Timusk, Appl. Opt. **32**, 2976 (1993).
[23] M. Dressel and G. Grüner, *Electrodynamics of Solids* (Cambridge University Press, Cambridge, England, 2001).
[24] A. Gozar and G. Blumberg, in *Frontiers in Magnetic Materials*, edited by A. V. Narlikar (Spinger-Verlag, Berlin, 2005) pp. 653–695; arXiv:cond-mat/0510193.
[25] D. König, U. Löw, S. Schmidt, H. Schwenk, M. Sieling, W. Palme, B. Wolf, G. Bruls, B. Lüthi, M. Matsuda, and K. Katsumata, Physica B (Amsterdam) **237–238**, 117 (1997).
[26] Y. Gotoh, I. Yamaguchi, Y. Takahashi, J. Akimoto, M. Goto, M. Onoda, H. Fujino, T. Nagata, and J. Akimitsu, Phys. Rev. B **68**, 224108 (2003).
[27] M. v. Zimmermann, J. Geck, S. Kiele, R. Klingeler, and B. Büchner, Phys. Rev. B **73**, 115121 (2006).